Monthly Notices
of the
ROYAL ASTRONOMICAL SOCIETY

MNRAS **496,** 784–800 (2020)
Advance Access publication 2020 May 30

doi:10.1093/mnras/staa1487

The nature of flux variations in the continua and broad-line regions of selected active galactic nuclei

A. Bewketu Belete,[1]★ L. J. Goicoechea,[2] B. L. Canto Martins,[1]★ I. C. Leão[1] and J. R. De Medeiros[1]

[1]*Departamento de Física Teórica e Experimental, Universidade Federal do Rio Grande do Norte, Natal, RN 59078-970, Brazil*
[2]*Departamento de Física Moderna, Universidad de Cantabria (UC), Avda. de Los Castros s/n, 39005 Santander, Spain*

Accepted 2020 May 20. Received 2020 May 20; in original form 2019 June 19

ABSTRACT

We present a multifractal analysis of the long-term light curves of a small sample of type 1 active galactic nuclei: NGC 4151, Arp 102B, 3C 390.3, E1821+643 and NGC 7469. We aim to investigate how the degrees of multifractality of the continuum and Hβ line vary among the five different objects and to check whether the multifractal behaviours of the continuum and the Hβ line correlate with standard accretion parameters. The backward ($\theta = 0$) one-dimensional multifractal detrended moving average procedure was applied to light curves covering the full observation period and partial observation periods containing an equal number of epochs for each object. We detected multifractal signatures for the continua of NGC 4151, Arp 102B and 3C 390.3 and for the Hβ lines of NGC 4151 and 3C 390.3. However, we found nearly monofractal signatures for the continua of E1821+643 and NGC 7469, as well as for the Hβ lines of Arp 102B, E1821+643 and NGC 7469. In addition, we did not find any correlations between the degree of multifractality of the Hβ line and accretion parameters, while the degree of multifractality of the continuum seems to correlate with the Eddington ratio (i.e. the smaller the ratio is, the stronger the degree of multifractality). The given method is not robust, and these results should be taken with caution. Future analysis of the sampling rate and other properties of the light curves should help with better constraining and understanding these results.

Key words: methods: statistical – galaxies: active – quasars: individual: NGC 4151 – quasars: individual: Arp 102B – quasars: individual: 3C 390.3 – quasars: individual: E1821+643 – quasars: individual: NGC 7469.

1 INTRODUCTION

The continuum region and broad-line region (BLR) are important components in active galactic nuclei (AGNs). The BLR is responsible for the formation of broad emission lines (BELs). One of the characteristics of the BELs in AGN spectra is the variations they exhibit in their flux in response to continuum variations on timescales of days to many weeks or longer. It has long been known that the continua of most AGNs change with time. It has been indicated that photoionization is the most likely mechanism for the generation of emission lines in AGNs, and thus a change in the ionizing continuum is expected to produce similar changes in the emission lines (Netzer 1990). Additionally, the application of the reverberation mapping technique, which is considered a standard tool for probing the structure and kinematics of the BLR in AGNs, to estimate the BLR radius is based on the assumption that the BLR is photoionized by the ionizing continuum from a central source (e.g. Peterson 1993, 2014). From the optical monitoring of AGNs, it has been shown that a time lag in the response of the BEL fluxes to a change in the continuum flux depends on the size, geometry and physical conditions of the BLR (Shapovalova et al. 2010b, 2013). Cross-correlating the broad-line and continuum light curves is a simple technique for determining the time lag between the line and continuum and for estimating the size/dimension of the line-emitting region. However, it is necessary to know the behaviour of the continuum light curve and the responses (linear or non-linear) of the lines, because the cross-correlation peak position depends on these two aspects (Netzer 1990).

It has been indicated that an understanding of the nature of flux variations in the continuum and BEL profiles and their correlations can provide us with potentially significant information about the

★ E-mail: asnakew@fisica.ufrn.br (ABB); brunocanto@fisica.ufrn.br (BLCM)

Table 1. Spectral characteristics of each source (see table 1 of Ilić et al. 2017, and references therein) and the results obtained from our multifractality analysis. The columns are as follows: (1) source name; (2) mass of the supermassive black hole $M_{\rm BH}$ in solar mass units ($M_\odot$); (3) mean continuum luminosity at 5100 Å (in 10^{44} erg s^{-1}); (4) BLR radius $c\tau_{\rm BLR}$ of the Hβ line (in d); (5) fractional variability amplitude (per cent) of the continuum at 5100 Å for the full (F_v) and partial ($F_v^{\rm p}$) observing periods; (6) fractional variability amplitude (per cent) of the Hβ line for the full (F_v) and partial ($F_v^{\rm p}$) observing periods (for F_v we use only two decimal places); (7) spectral width (5100 Å) for the full observing period; (8) spectral width (Hβ) for the full observing period; (9) spectral width (5100 Å) for the partial observing period; (10) spectral width (Hβ) for the partial observing period. All the widths of the spectrum functions are rounded to three decimal places.

Object	$M_{\rm BH}$	λL_λ	$c\tau_{\rm BLR}$	$(F_v/F_v^{\rm p})_{\rm cnt}$	$(F_v/F_v^{\rm p})_{\rm H\beta}$	$\Delta\alpha_{5100}$(f)	$\Delta\alpha_{H\beta}$(f)	$\Delta\alpha_{5100}$(p)	$\Delta\alpha_{H\beta}$(p)
NGC 4151	1.6×10^8	0.05 ± 0.03	5^{+28}_{-5}	0.59/0.56	0.42/0.41	0.548 ± 0.021	0.235 ± 0.014	0.186 ± 0.004	0.226 ± 0.015
Arp 102B	1.1×10^8	0.11 ± 0.01	15^{+20}_{-15}	0.31/0.30	0.11/0.10	0.28 ± 0.020	0.039 ± 0.006	0.134 ± 0.002	0.024 ± 0.003
Arp 102B (Hβ)b					0.20/0.19		0.190 ± 0.010		0.080 ± 0.003
Arp 102B (Hβ)c					0.14/0.11		0.057 ± 0.005		0.030 ± 0.001
Arp 102B (Hβ)r					0.13/0.12		0.051 ± 0.003		0.044 ± 0.006
3C 390.3	2.1×10^9	0.90 ± 0.42	96^{+28}_{-47}	0.46/0.42	0.38/0.32	0.248 ± 0.009	0.323 ± 0.044	0.118 ± 0.005	0.778 ± 0.043
E1821+643	2.6×10^9	104.4 ± 19.9	$118^{+0.1}_{-0.0}$	0.19/0.19	0.07/0.07	0.064 ± 0.002	0.003 ± 0.000	0.062 ± 0.001	0.002 ± 0
E1821+643 (Hβ)b					0.17/0.17		0.018 ± 0.001		0.036 ± 0.005
E1821+643 (Hβ)c					0.12/0.13		0.006 ± 0.000		0.022 ± 0.004
E1821+643 (Hβ)r					0.11/0.14		0.003 ± 0.000		0.044 ± 0.007
NGC 7469	1.1×10^7	0.52 ± 0.08	5^{+7}_{-0}	0.15/0.15	0.23/0.20	0.025 ± 0.001	0.084 ± 0.005	0.015 ± 0.000	0.107 ± 0.006

physics of the BLR cloud system and about the central engine (e.g. Peterson 1993, and references therein; Shapovalova et al. 2009).

In the study of the variability of AGNs, the most common techniques, including the power spectrum, structure function, rescaled range and periodiogram methods, are either inconsistently appropriate or limited in their ability to characterize the variability mechanisms as these approaches are mostly suitable for linear/Gaussian processes (Vio et al. 1992). Longo et al. (1996) studied the non-linear variability of NGC 4151 and concluded that linear models cannot account for the characteristics of the source light curves. In addition, Vio et al. (1991) studied the optical light curve of the optically violent variable quasar 3C 345 and showed that the curve cannot be regenerated by linear processes. In general, because AGNs are complex and chaotic systems, it is more appropriate to employ non-linear techniques to study their variability and to understand the physics behind them (e.g. Vio et al. 1992; Chian 1997).

Here, we study the multifractal and thus non-linear behaviour of the flux variations in the long-term optical light curves (i.e. the continuum and Hβ line) of selected AGNs, such as NGC 4151, Arp 102B, 3C 390.3, E1821+643 and NGC 7469. These objects are selected to make use of the advantage that they have long-term optical light curves (the continuum at 5100 Å and the Hβ line), which were homogeneously obtained and analysed by the same research group (see Shapovalova et al. 2008, 2010a, b, 2013, 2016, 2017, and references therein). We apply the multifractal detrended moving average (MFDMA) algorithm, particularly the one-dimensional backward MFDMA (see Gu & Zhou 2010; Bewketu Belete et al. 2019c). The MFDMA technique is an extension of the detrended moving average, which in turn is a modification of detrended fluctuation analysis (see Bewketu Belete et al. 2019c, and references therein). This technique has been applied to different science cases within fields as disparate as economics (e.g. Gu & Zhou 2010; Wang, Wu & Pan 2011) and astrophysics. By using hourly time series extracted from the *CoRoT* data base, de Freitas et al. (2016) have shown that the rotation period of a star is inherently scaled by the degree of multifractality; see also de Freitas et al. (2019) for an analysis of *Kepler* stars. Bewketu Belete et al. (2018) were the first to use the MFDMA technique to study AGN time series. Most recently, we have analysed the long-term (45 yr) optical (i.e. continuum at 5100 Å and Hβ line) light curves of the Seyfert 1 galaxy NGC 5548 and we have shown that the non-linearity of the Hβ line is approximately twice as high as that of the continuum (Bewketu Belete et al. 2019c). This could be interpreted as a dilution effect; that is, all Hβ emissions are generated in the BLR after the reprocessing of the nuclear continuum, while only a fraction of the continuum comes from BLR clouds.

As shown in Table 1, the candidate AGNs are different in many aspects, such as their black hole mass, variability amplitude, continuum luminosity and the size of their BLR. NGC 4151 is a well-known type 1 AGN with a redshift of 0.0033 (Kovačević et al. 2018, and references therein). Through multifractal analysis, Longo et al. (1996) found non-linear and intermittent behaviour in the long-term (1910–1991) *B*-band light curve of NGC 4151. Shapovalova et al. (2008) studied the long-term (1996–2006) variability of the optical spectra of NGC 4151 and found strong variability in the 5100-Å continuum and Hβ line fluxes; they also found that the variability amplitude of the continuum flux is greater than that of the line. In addition, during the period 2000–2006, when the continuum flux was small, they found good correlation between the Hβ line flux and the continuum flux and they showed that the line was generated by photoionization of the optical continuum. However, Shapovalova et al. (2008) also indicated that when the whole monitoring period is considered (especially periods with high continuum flux), the line flux correlates very weakly with the continuum, raising questions about this photoionization assumption. The optical variability of NGC 4151 has been studied by many different authors (e.g. Beall et al. 1981; Antonucci & Cohen 1983; Maoz et al. 1991; Alexander et al. 1999; Ulrich 2000; Pronik & Sergeeva 2001; Fan, Su & Lin 2002; Czerny et al. 2003; Guo, Tao & Qian 2006; Rakić et al. 2017; Kovačević et al. 2018; and references therein).

Arp 102B, at a redshift of 0.024 (Shapovalova et al. 2013; Kovačević et al. 2018), is a type of AGN with double-peaked BELs that are thought to be emitted from an accretion disc (Gezari, Halpern & Eracleous 2007). Arp 102B is the first AGN to which an accretion-disc BLR geometry has been applied (Chen & Halpern 1989; Chen, Halpern & Filippenko 1989). Using long-term (1987–2010) optical spectral observations of Arp 102B, Shapovalova et al. (2013) studied the variability in the spectral lines and continuum

flux. They found a weak correlation between the emission line and continuum flux variations, indicating that the line variation is weakly associated with the variation in the central photoionization source. Although the fluxes in the lines and in the continuum showed no significant change (∼20 per cent) during the monitored period, Shapovalova et al. (2013) demonstrated that the variability amplitude of the continuum (5100 Å) is significantly greater than that of the Hβ line after subtracting the host-galaxy contribution; however, with the host-galaxy contribution, the variability amplitude of the line was shown to be greater than that of the continuum. Popović et al. (2014) also studied the long-term (1987–2013) variability in the broad-line profiles of radio galaxy Arp 102B. They concluded that the BLR of Arp 102B may have a disc-like geometry and that the variations in the properties of the broad-line profiles may be partly due to an outflow. However, Popović et al. (2014) indicated that the observed variability in the line parameters is not in good agreement with the disc hypothesis of the line-emitting region. Several studies have been conducted on the optical variability of Arp 102B (e.g. Antonucci, Hurt & Agol 1996; Newman et al. 1997; Gezari et al. 2004, 2007; Rakić et al. 2017; Kovačević et al. 2018; and references therein).

3C 390.3 is broad-line radio galaxy at a redshift of 0.0561 (Shapovalova et al. 2010b; Kovačević et al. 2018). The nucleus of 3C 390.3 has double-peaked BELs thought to be emitted from an accretion disc. The optical continuum and emission-line fluxes of this AGN have been shown to be strongly variable (e.g. Yee & Oke 1981; Wamsteker et al. 1997; Shapovalova et al. 2001; Sergeev et al. 2002; Tao et al. 2008). Popović et al. (2011) investigated the variability of the BEL profiles and the *H*α and Hβ lines of 3C 390.3 during 1995–2007 and claimed that the variations in the line profiles correspond to the emission of a disc-like BLR. They also indicated that the geometry of the source BLR seems to be very complex and that the BLR with its disc-like geometry is the dominant emitter. In addition, Shapovalova et al. (2010b) studied long-term (1995–2007) optical observations of 3C 390.3 and found that the broad emission components of the Hα and Hβ lines and the continuum flux varied by a factor of ≈4–5. They also determined time lags of ∼95 d between the continuum and Hβ flux and approximately 120 d between the continuum and Hα line flux. See also Barr et al. (1980), Yee & Oke (1981), Netzer (1982), Veilleux & Zheng (1991), Zheng (1996), Die (1998), Shapovalova et al. (2001), Sergeev et al. (2011), Dietrich et al. (2012), Sergeev, Nazarov & Borman (2017), Rakić et al. (2017), Kovačević et al. (2018), and references therein.

The quasar E1821+643, at a redshift of 0.297, has strong red asymmetry and a blueshifted peak in its line profiles and it is one of the most luminous radio-quiet quasars in the Local Universe (Shapovalova et al. 2016). Shapovalova et al. (2016) studied the long-term (1990–2014) variability of E1821+643 in the continua (4200 and 5100 Å) and BELs (Hβ and Hγ) and found significant changes in the continua and Hγ line but smaller variations in the Hβ line during the monitored period. The variability amplitude of the continuum at 5100 Å is greater than that of the Hβ line, whereas the variability amplitude of the continuum at 4200 Å is almost equal to that of the Hγ line. See also Kolman et al. (1991, 1993), Oegerle et al. (2000), Blundell & Rawlings (2001), Kollatschny, Zetzl & Dietrich (2006), Landt et al. (2008), Walker et al. (2014), Kovačević et al. (2017, 2018), Rakić et al. (2017), and references therein.

NGC 7469, at a redshift of 0.0163 (see table 1 of Ilić et al. 2017), is a type 1 AGN that shows significant variability in the continuum and line spectra (Shapovalova et al. 2017). Dultzin-Hacyan et al. (1992) performed optical monitoring of NGC 7469 over 13 photometric nights (November 3–30) and concluded that random variability was present during the first four nights with an average amplitude of approximately 0.040 m, for an average time-scale of approximately 13 min. They also indicated that the observed random variability could be due to local instabilities in the accretion disc. Dultzin-Hacyan, Ruelas-Mayorga & Costero (1993) also performed optical monitoring of NGC 7469 over four nights in search of microvariability, but they did not detect this phenomenon during the 4-d monitoring period. Recently, by using long-term (1996–2015) photometric and spectroscopic observations of NGC 7469, Shapovalova et al. (2017) investigated the long-term variability in the continuum, BEL fluxes and broad-line profiles of NGC 7469 and they found that the variability amplitude of the Hβ broad line (∼23 per cent) is greater than that of the continuum at 5100 Å (∼14 per cent). Additionally, they found very strong correlations between the line and the continuum flux, indicating that the BLR gas cloud is most likely photoionized by the central continuum source. See also Welsh et al. (1998), Petrucci et al. (2004), Doroshenko et al. (2010), Peterson et al. (2014), Baldi et al. (2015), Mehdipour et al. (2018), Middei et al. (2018), Seifina, Titarchuk & Ugolkova (2018), and references therein.

This work is intended to address three questions. Are the responses of BELs to variations in the ionizing continuum the same for all AGNs? Is the degree of multifractality (non-linearity) of the continuum of an AGN dependent on the black hole mass, on the continuum luminosity or on the Eddington ratio? Is the degree of multifractality of BELs of AGNs dependent on the black hole mass, on the size of the BLR or on the continuum luminosity? The remainder of this work is organized as follows. In Section 2, we present the data and explain the procedures followed. The results and discussion are provided in Section 3. The main conclusions are provided in Section 4.

2 OBSERVATIONAL DATA AND ANALYSIS METHOD

2.1 Light curves

In this work, we use the long-term optical light curves of NGC 4151 (see the top-left panel of Fig. 1; Shapovalova et al. 2010a, 2008), Arp 102B (see the top-right panel of Fig. 1; Shapovalova et al. 2013), 3C 390.3 (see the middle-left panel of Fig. 1; Shapovalova et al. 2010b), E1821+643 (see the middle-right panel of Fig. 1; Shapovalova et al. 2016) and NGC 7469 (see the bottom panel of Fig. 1; Shapovalova et al. 2017). For Arp 102B, we use host-galaxy-corrected data. In addition, we also use the Hβ line segments of Arp 102B (see the left panel of Fig. 2; Shapovalova et al. 2013) and E1821+643 (see the right panel of Fig. 2; Shapovalova et al. 2016). We consider two sets of light curves with different lengths: (i) full observing period light curves and (ii) partial observing period light curves containing an equal number of epochs. The number of data points and the sampling rates for the full and partial observation periods are given in Table 2.

2.2 Procedures for analysing light curves

We applied the backward ($\theta = 0$) one-dimensional MFDMA algorithm discussed in Bewketu Belete et al. (2019c) and references therein. This multifractality analysis technique allows us to determine the most important parameters that can be used to describe

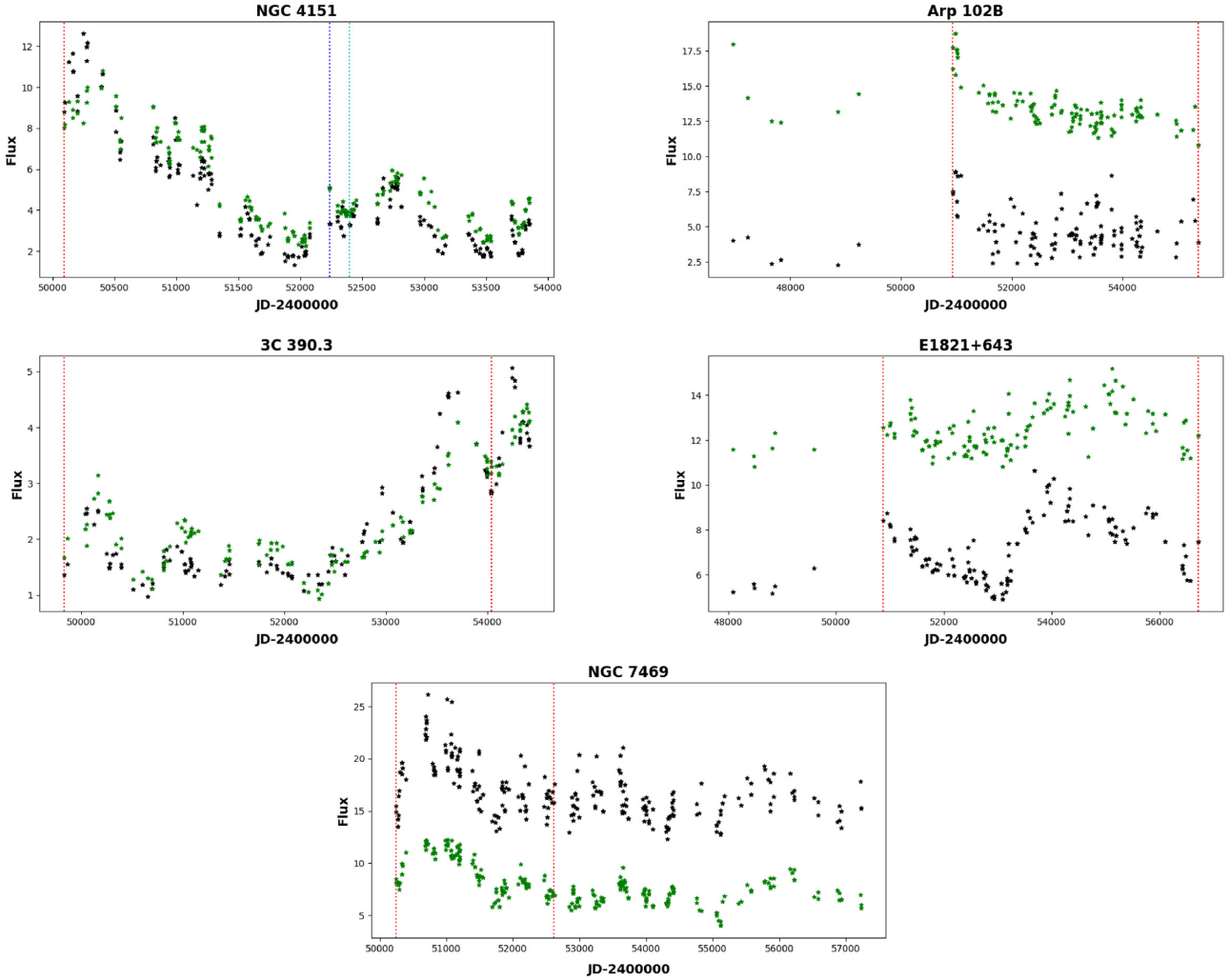

Figure 1. The continuum at 5100 Å (black) and the Hβ line (green) light curves of NGC 4151 (top-left panel), Arp 102B (top-right panel), 3C 390.3 (middle-left panel), E1821+643 (middle-right panel) and NGC 7469 (bottom panel). Vertical dashed lines indicate the start and end dates of the partial light curves containing an equal number of epochs for all objects, i.e. 110 epochs with mean sampling rates ranging from 0.67 (E1821+643) to 1.56 (NGC 4151) points per month. We also note that the partial light curves for Arp 102B and E1821+643 are associated with densely sampled periods. The continuum and Hβ ending dates for NGC 4151 do not coincide; thus, two vertical lines of different colours were used (a blue dashed line for 5100 Å and a cyan dashed line for Hβ). The fluxes are given in 10^{-15} erg cm^{-2} s^{-1} Å^{-1} (continuum at 5100 Å) and 10^{-13} erg cm^{-2} s^{-1} (Hβ line).

Table 2. The columns are as follows: (1) source name; (2) number of data points (full observing period; 5100 Å); (3) number of data points (full observing period; Hβ); (4) sampling rate (full observing period; 5100 Å); (5) sampling rate (full observing period; Hβ); (6) number of data points (partial observing period; 5100 Å); (7) number of data points (partial observing period; Hβ); (8) sampling rate (partial observing period; 5100 Å); (9) sampling rate (partial observing period; Hβ). The sampling rate is the number of data points per day.

Object	N_f(5100 Å)	N_f(Hβ)	S_f(5100 Å)	S_f(Hβ)	N_p(5100 Å)	N_p(Hβ)	S_p(5100 Å)	S_p(Hβ)
NGC 4151	220	180	0.0586	0.048	110	110	0.05	0.0478
Arp 102B	116	118	0.0138	0.014	110	110	0.0248	0.0248
3C 390.3	128	129	0.0279	0.028	110	110	0.0304	0.0307
E1821+643	127	127	0.0217	0.0217	110	110	0.022	0.022
NGC 7469	233	233	0.0334	0.0334	110	110	0.0464	0.0464

the behaviours of variations (the scaling nature) in the light curves considered herein. These parameters are as follows: a qth-order overall fluctuation function $Fq(n)$, where n is the segment size series (a set or an array of window size) and q is the statistical moment; the classic scaling exponent $\tau(q)$; the multifractal spectrum function $f(\alpha)$, where α is the singularity strength. The lower limit (n_{min}) of the segment size is approximately 10, and the upper limit (n_{max}) of the segment size is approximately 10 per cent of the length

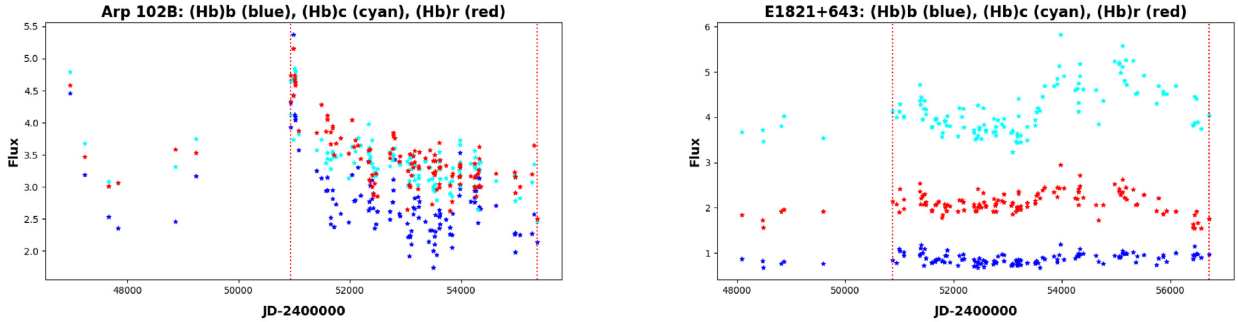

Figure 2. The same as in Fig. 1 but for the Hβ line segments: the blue wing (Hβ)b (blue), line core (Hβ)c (cyan) and red wing (Hβ)r (red), of Arp 102B (left) and E1821+643 (right).

of the time series considered. The procedures are summarized as follows. First, we reconstructed the time series x(t) as a sequence of cumulative sums $y(t) = \sum_{i=1}^{t} x(i), \quad t = 1, 2, 3, ..., N$, where N is the length of the time series. Second, we calculated the moving average function in a moving window. Third, we removed the trend from the reconstructed time series and obtained the residual sequence. Fourth, we calculated the root-mean-square function. Fifth, we determined the overall fluctuation function $Fq(n)$. Sixth, using the least-squares fitting technique, we calculated the slope $h(q)$, usually known as the local Hurst exponent for a multifractal time series (Hampson & Mallen 2011), from the log–log plot of $Fq(n)$ versus n for each statistical moment q. Seventh, we estimated the classic scaling exponent function, known as the Renyi scaling exponent, $\tau(q)$, which reflects how the overall fluctuation function $Fq(n)$ scales at each local scale n for each q. Finally, we estimated the multifractal spectrum function $f(\alpha)$ and calculated the width ($\Delta\alpha = \alpha_{\max} - \alpha_{min}$) of the spectra.

3 RESULTS

We analysed the multifractal (non-linear) properties of the long-term optical spectra, namely, the continuum (5100 Å) and Hβ line, of the selected type 1 AGNs, using the backward one-dimensional MFDMA analysis procedure. The results obtained – the overall fluctuation function $Fq(n)$, the local Hurst exponent $h(q)$ or slope, the classic scaling exponent $\tau(q)$ and the multifractal spectrum function $f(\alpha)$ – are given in Fig. 3 for NGC 4151, in Figs 4 and 5 for Arp 102B, in Fig. 6 for 3C 390.3, in Figs 7 and 8 for E1821+643 and in Fig. 9 for NGC 7469. Table 1 summarizes the following spectral characteristics of each source (from left to right) and the results obtained from our multifractality analysis: the source name, mass of the supermassive black hole $M_{\rm BH}$, mean continuum luminosity at 5100 Å, BLR radius $c\tau_{BLR}$ of the Hβ line, fractional variability amplitude of the continuum at 5100 Å for the full and partial observing periods, fractional variability amplitude of the Hβ line for the full and partial observing periods, spectral width (5100 Å) for the full observing period, spectral width (Hβ) for the full observing period, spectral width (5100 Å) for the partial observing period, and spectral width (Hβ) for the partial observing period. We estimated the fractional variability amplitude F_v as (Edelson et al. 2019)

$$F_v = \Delta F / \langle F \rangle, \tag{1}$$

where $\Delta F = (\sigma_F^2 - e_F^2)^{1/2}$, σ_F^2 and $\langle F \rangle$ are the total variance and mean, respectively, of the light curve, and e_F^2 is the mean error.

For a multifractal time series, the overall fluctuation function $Fq(n)$ looks different for the negative and positive q at the smallest scale n relative to the largest scale (Ihlen 2012). In addition, the functional relationship between the statistical moment q and the slope $h(q)$ calculated from the log–log plot of $Fq(n)$ and n further describes the nature of the overall fluctuation functions for positive and negative values of q. Furthermore, for a multifractal signal, the slope $h(q)$ decreases with q (Tanna & Pathak 2014). In contrast, for a monofractal time series, $Fq(n)$ does not appear different for positive and negative q, and consequently the slope $h(q)$ will have a constant value; that is, $h(q)$ does not change with the moment q (Kantelhardt et al. 2002). Because the classic scaling exponent $\tau(q)$ is a reflection of the local Hurst exponent $h(q)$, for a multifractal time series, $\tau(q)$ shows non-linear dependence on q, whereas it shows no dependence on q if the time series has a monofractal nature (e.g. Kantelhardt et al. 2002; Hampson & Mallen 2011; Ihlen 2012; Tanna & Pathak 2014). It has been shown that the width and shape of a multifractal spectrum are related to the temporal variation of the local Hurst exponent $h(q)$. The width ($\Delta\alpha = \alpha_{\max} - \alpha_{\min}$) of the multifractal spectrum is a measure of the degree of multifractality detected in a given time series (Ashkenazy et al. 2003), where wider widths indicate stronger multifractality (Kantelhardt et al. 2002). The shape of a multifractal spectrum presents three types of symmetry: left-side truncation, right-side truncation and symmetric. A multifractal spectrum is found to be left-side truncated if the multifractality is sensitive to local small-magnitude fluctuations, or right-side truncated if the multifractality is sensitive to local large-magnitude fluctuations (see Bewketu Belete et al. 2018, and references therein).

3.1 NGC 4151

As can be seen in the top and first middle panels of Fig. 3, the overall fluctuation functions $Fq(n)$ for both the continuum (5100 Å) and the Hβ line look different for positive and negative q. Additionally, the slope (the local Hurst exponent) $h(q)$, as shown in the second middle-left panel in Fig. 3, is strongly dependent on the moment q and decreases with q. These behaviours of $Fq(n)$ and $h(q)$ indicate the presence of a multifractal (non-linear) signature in the continuum and Hβ line flux observations of NGC 4151. In addition, the corresponding classic scaling exponent functions $\tau(q)$ are non-linear functions of q; that is, $\tau(q)$ has a different slope for positive and negative q (see the second middle-right panel in Fig. 3). The evolution of $h(q)$ with q and the degree of non-linearity in $\tau(q)$ are different between the continuum and Hβ line, indicating that the degree of multifractality between them is different. We

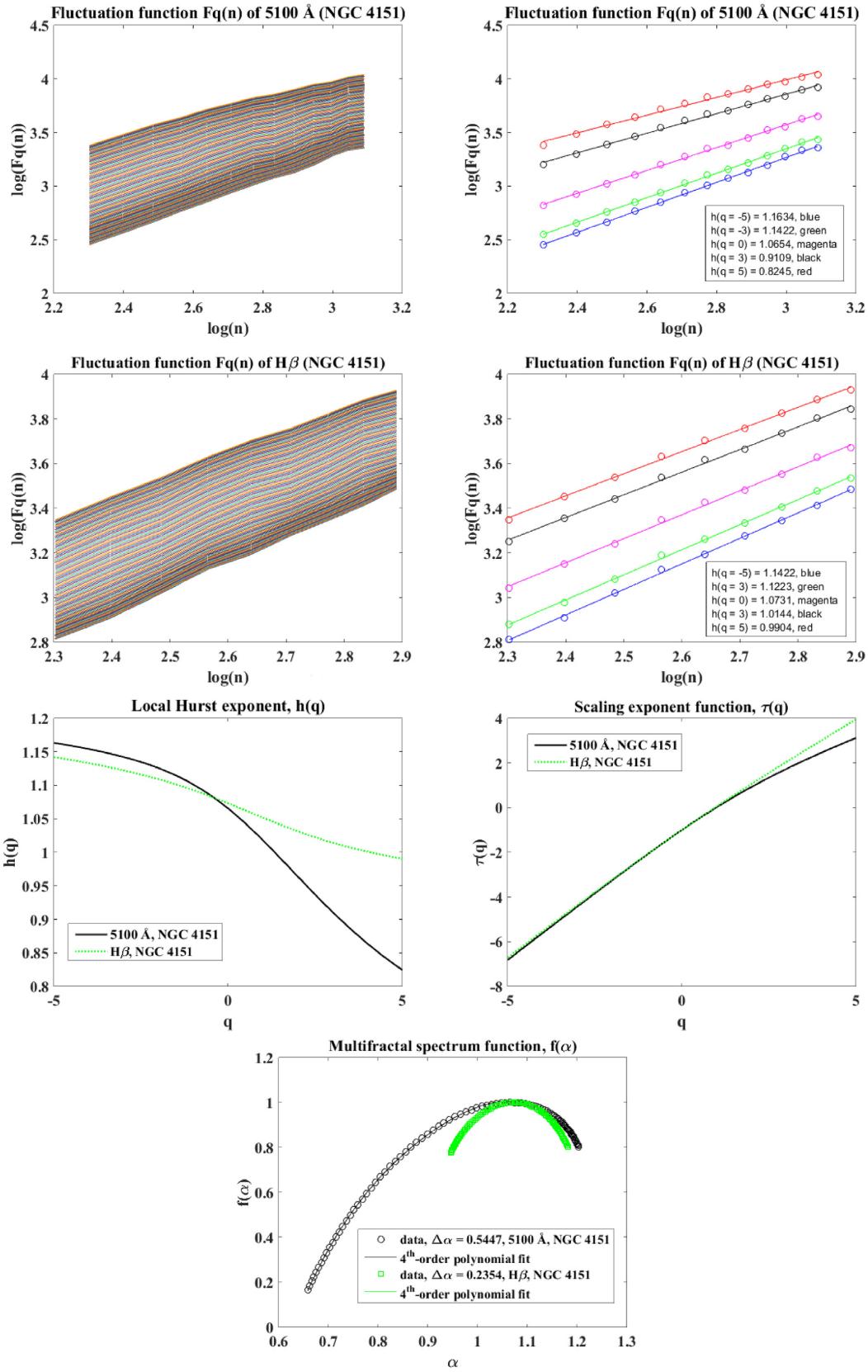

Figure 3. Top panels: the overall fluctuation functions $Fq(n)$ (left) and the fitted overall fluctuation functions for different Hurst exponents denoted with different colours (right) for the continuum of NGC 4151. First middle panels: the same as the top panels but for the Hβ line. Second middle panels: the local Hurst exponents $h(q)$ (left) for the continuum (black solid line) and Hβ line (green dots) and the scaling exponent functions $\tau(q)$ (right) for the continuum (black solid line) and Hβ line (green dots). Bottom panel: the multifractal spectrum functions for the observed continuum (black circle) and Hβ line (green square) fitted with a fourth-order polynomial function (solid lines). The width $\Delta\alpha$ of both spectrum functions is also given.

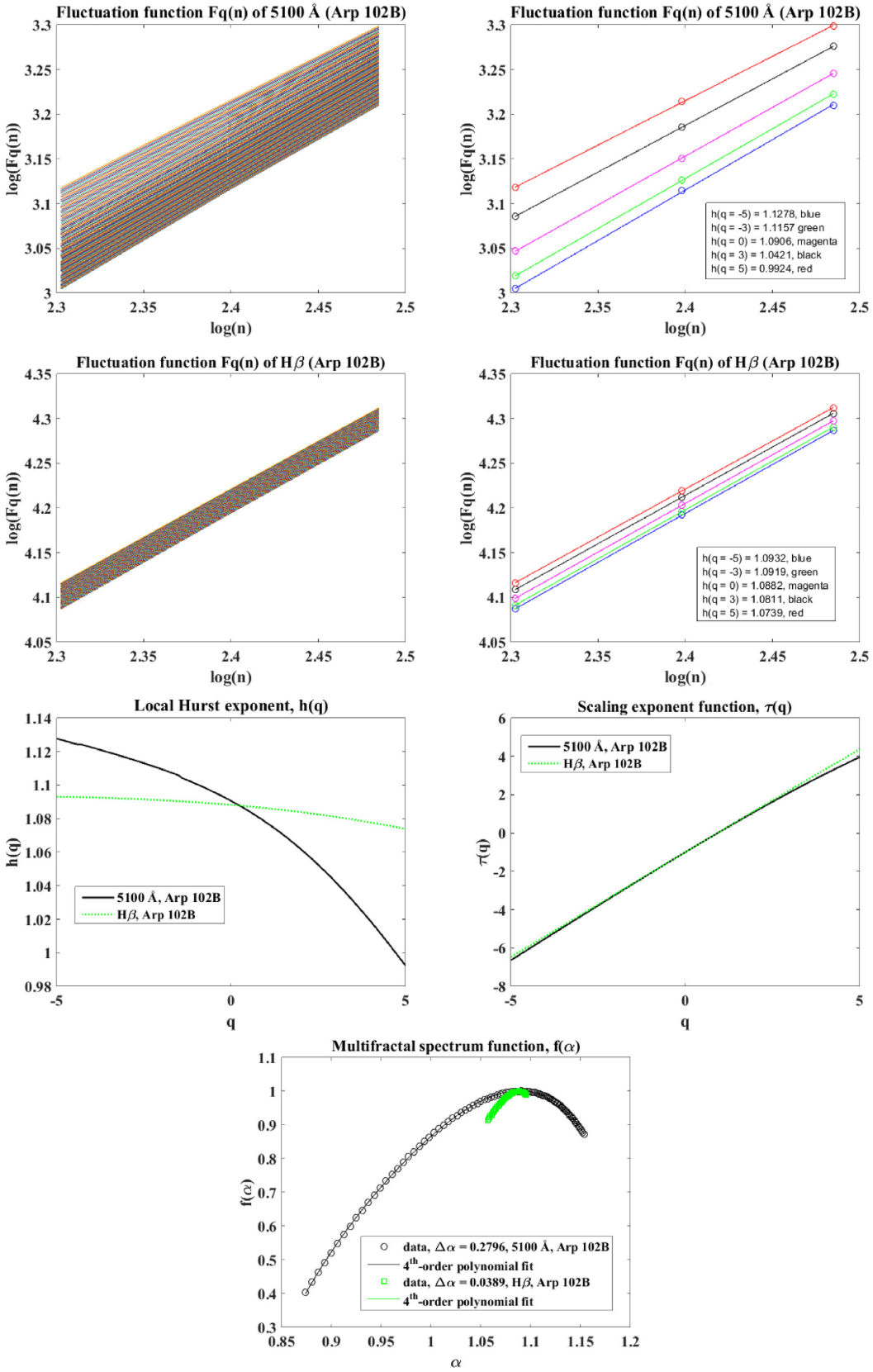

Figure 4. Top panels: the overall fluctuation functions $Fq(n)$ (left) and the fitted overall fluctuation functions for different Hurst exponents denoted with different colours (right) for the continuum of Arp 102B. First middle panels: the same as the top panels but for the Hβ line. Second middle panels: the local Hurst exponents $h(q)$ (left) for the continuum (black solid line) and Hβ line (green dots) and the scaling exponent functions $\tau(q)$ (right) for the continuum (black solid line) and Hβ line (green dots). Bottom panel: the multifractal spectrum functions for the observed continuum (black circle) and Hβ line (green square) fitted with a fourth-order polynomial function (solid lines). The width $\Delta\alpha$ of both spectrum functions is also given.

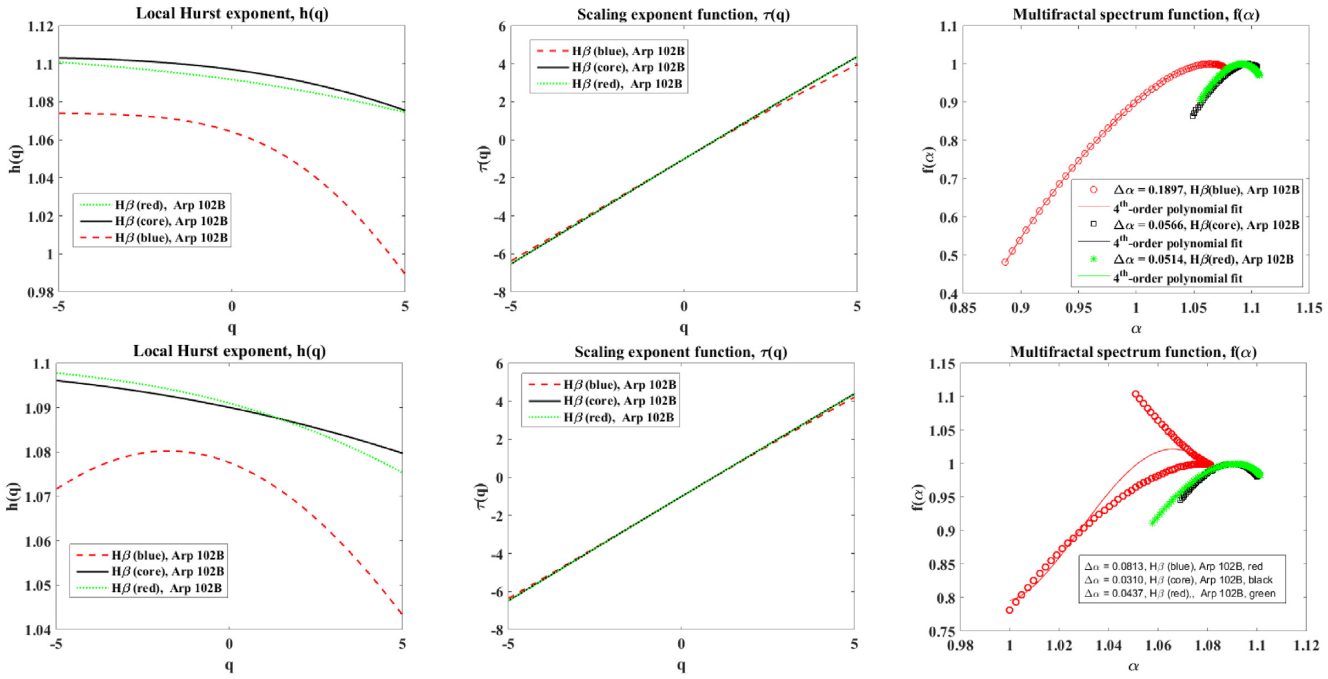

Figure 5. Top panels: the local Hurst exponents (left), the scaling exponent functions (middle) and the multifractal spectrum functions (right) for the full observation period of the Hβ line segments of Arp 102B: (Hβ)b (red dashed line), (Hβ)c (black solid line) and (Hβ)r (green dots). Bottom panels: The same as the top panels but for the partial observation period (from day 50940.34 to day 55367.42).

estimated the shapes and widths of the multifractal spectra (see the bottom panel in Fig. 3). The widths of the multifractal spectra can be calculated as $\Delta\alpha = \alpha_{\max} - \alpha_{\min}$: 0.5447 (5100 Å) and 0.2354 (Hβ). These widths further confirm the above discussion based on $Fq(n)$, $h(q)$ and $\tau(q)$ in that there are strong multifractal signatures in both the continuum and the Hβ line light curves. However, the degree of multifractality of the continuum (5100 Å) is greater than that of the Hβ line ($\Delta\alpha_{5100\,\text{Å}} > \Delta\alpha_{\text{H}\beta}$). The shapes of the spectra for both the continuum and the line are found to be right-side truncated, meaning that the detected multifractality is sensitive to local large-magnitude fluctuations. Observational uncertainties (noise) could contribute to the wide widths (Bewketu Belete et al. 2018). Thus, to take into account this effect, we generated simulated light curves of the continuum and Hβ line at epochs equal to those of observations and modified the observed fluxes by adding random quantities. These additive random numbers were normally distributed around zero with standard deviations equal to the measured uncertainties. Our analysis method was then applied to the simulated curves to produce distributions of the spectral shapes and widths. We found identical spectral shapes and small differences in the widths after observational noise was taken into account. The small differences in the spectral width allowed us to infer the 1σ errors shown in Table 1.

3.2 Arp 102B

The overall fluctuation functions $Fq(n)$, the slope $h(q)$, the scaling exponent functions $\tau(q)$ and the multifractal spectra $f(\alpha)$ for the continuum at 5100 Å and the Hβ line (host-galaxy-corrected) are given in the top and first middle panels, second middle-left panel, second middle-right panel and bottom panel, respectively, in Fig. 4. In addition, in Fig. 5, we present the Hurst exponents $h(q)$ (top-left panel), the scaling exponent functions $\tau(q)$ (top-middle panel) and the multifractal spectrum functions $f(\alpha)$ (top-right panel) for the full observation period of the core and the two wings of the Hβ line, i.e. Hβ (blue), Hβ (core) and Hβ (red). As is clearly explained earlier in Section 3, the behaviours of $Fq(n)$ and $h(q)$ and the width $\Delta\alpha$ reveal the presence of multifractal signatures in the continuum (5100 Å) and in Hβ (blue) and nearly monofractal signatures in the Hβ line, Hβ (core) and Hβ (red). This is because for truly monofractal data, $h(q)$ is expected to be the same for all q, and consequently the spectrum width would be 0. The difference in $\Delta\alpha$ between the continuum (5100 Å) and Hβ (blue) shows the difference in the degree of multifractality present in the corresponding time series. The spectrum of both the continuum and the Hβ (blue) wing is right-side truncated, indicating the sensitivity of the multifractality to local large-magnitude fluctuations. We take into account the effects of flux uncertainties on the widths and shapes of the spectra. Although the shapes of the spectra do not change, we found small differences in the widths of the spectra. The small differences in the width allowed us to infer 1σ confidence intervals (see Table 1). The widths show that the degree of multifractality of the continuum is significantly (several times) greater than that of the line.

3.3 3C 390.3

The overall fluctuation functions $Fq(n)$, the local Hurst exponents $h(q)$, the scaling exponent functions $\tau(q)$ and the widths of the multifractal spectra $f(\alpha)$ for the continuum at 5100Å and the Hβ line of 3C 390.3 are shown in Fig. 6. $Fq(n)$ is different for positive and negative q, which is the behaviour of $Fq(n)$ for a multifractal time series. In addition, the slopes $h(q)$ for the continuum and the line are shown to be decreasing functions of the moment q. Consequently, $\tau(q)$ is a non-linear function of q; i.e. $\tau(q)$ takes different values for positive and negative q, indicating the multifractal behaviours of the continuum and the line. However, as shown in Fig. 6, the degree

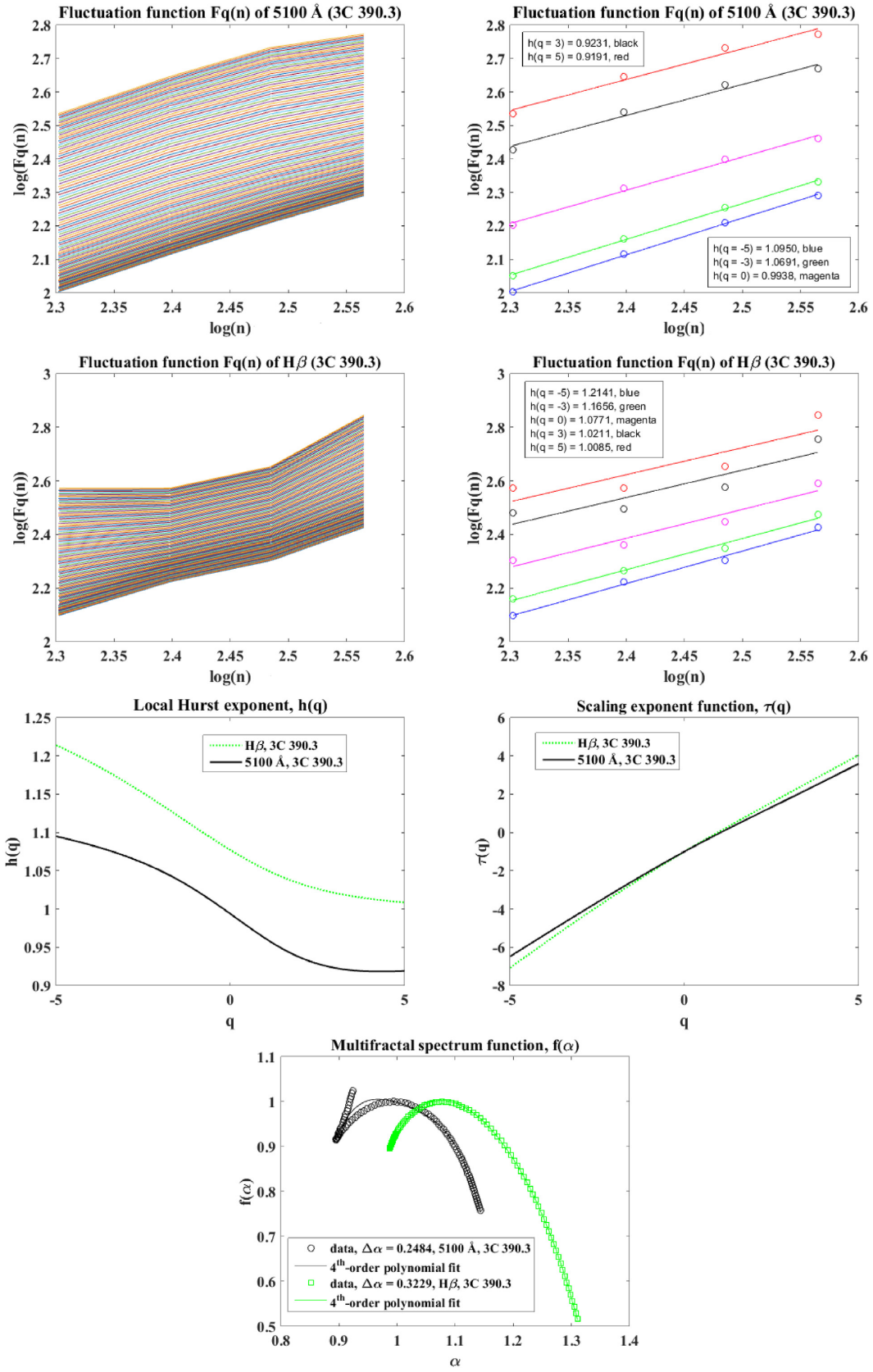

Figure 6. Top panels: the overall fluctuation functions $Fq(n)$ (left) and the fitted overall fluctuation functions for different Hurst exponents denoted with different colours (right) for the continuum of 3C 390.3. First middle panels: the same as the top panels but for the Hβ line. Second middle panels: the local Hurst exponents $h(q)$ (left) for the continuum (black solid line) and Hβ line (green dots) and the scaling exponent functions $\tau(q)$ (right) for the continuum (black solid line) and Hβ line (green dots). Bottom panel: the multifractal spectrum functions for the observed continuum (black circle) and Hβ line (green square) fitted with a fourth-order polynomial function (solid lines). The width $\Delta\alpha$ of both spectrum functions is also given.

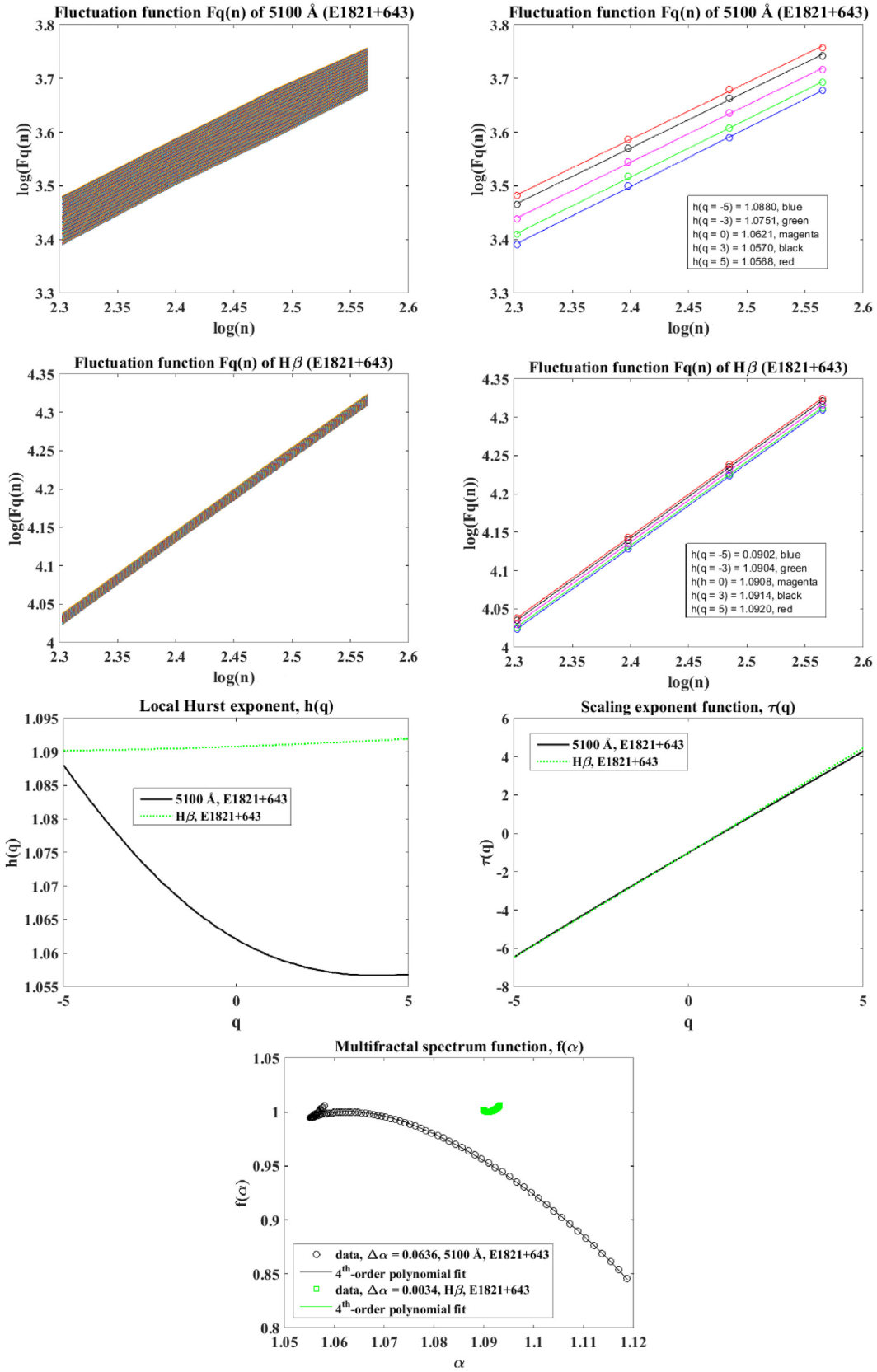

Figure 7. Top panels: the overall fluctuation functions $Fq(n)$ (left) and the fitted overall fluctuation functions for different Hurst exponents denoted with different colours (right) for the continuum of E1821+643. First middle panels: the same as the top panels but for the Hβ line. Second middle panels: the local Hurst exponents $h(q)$ (left) for the continuum (black solid line) and Hβ line (green dots) and the scaling exponent functions $\tau(q)$ (right) for the continuum (black solid line) and Hβ line (green dots). Bottom panel: the multifractal spectrum functions for the observed continuum (black circle) and Hβ line (green square) fitted with a fourth-order polynomial function (solid lines). The width $\Delta\alpha$ of both spectrum functions is also given.

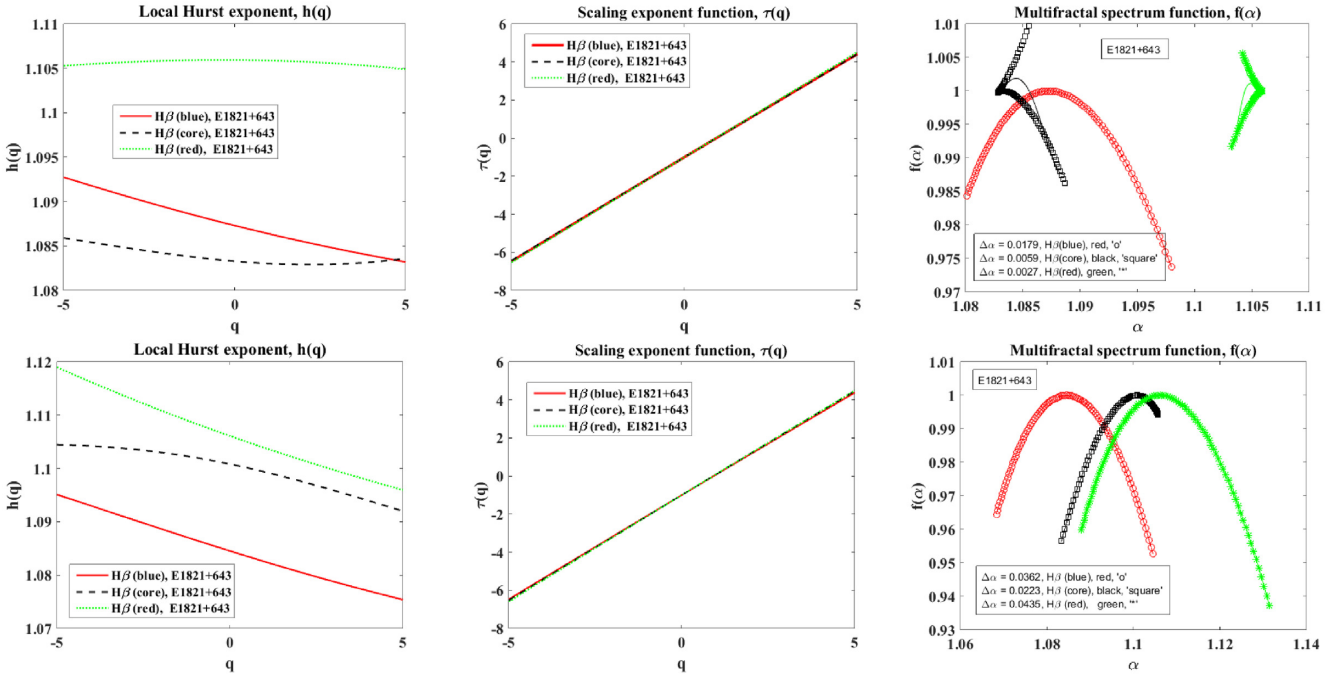

Figure 8. Top panels: the local Hurst exponents (left), the scaling exponent functions (middle) and the multifractal spectrum functions (right) for the full observation period of the Hβ line segments of E1821+643: (Hβ)b (red dashed line), (Hβ)c (black solid line) and (Hβ)r (green dots). Bottom panels: the same as the top panels but for the partial observation period (from day 50866.6 to day 55866.2).

of non-linearity in $\tau(q)$ is different between the continuum and the line. As noted, this difference in the non-linear behaviour of $\tau(q)$ clearly shows the difference in the degree of multifractality (non-linearity) between the continuum and the line. We can determine the degree of multifractality from the width of the spectra: $\Delta\alpha = 0.2484$ (5100 Å) and 0.3229 (Hβ). The shapes of the spectra are found to be left-side truncated, implying that the multifractality is sensitive to local small-magnitude fluctuations. Here, we also take into account the effects of flux uncertainties on the widths and shapes of the spectra. After taking these flux uncertainties into account, the spectral shapes are found to be identical, whereas the widths are changed by small values. The formal uncertainties are presented in Table 1. The spectral widths indicate that the degree of multifractality of the Hβ line is slightly greater than that of the continuum.

3.4 E1821+643

We performed the same multifractality analysis for the long-term optical light curves of E1821+643. The resulting $Fq(n)$, $h(q)$, $\tau(q)$ and $f(\alpha)$ for the continuum (5100 Å) and Hβ line of E1821+643 are given in Fig. 7. As shown in the top panels in Fig. 8, we also performed the same multifractality analysis for the full observation period of the different regions of the Hβ line segments: Hβ (blue), Hβ (core) and Hβ (red). After taking into account the flux uncertainties, the 1σ confidence intervals for the spectral widths are shown in Table 1. The behaviours of the overall fluctuation functions $Fq(n)$, slopes $h(q)$, scaling exponent functions $\tau(q)$ and spectral widths $\Delta\alpha$ clearly show the presence of monofractality in the flux observations of the Hβ line and the Hβ line segments and a very weak multifractal (nearly monofractal) signature of the continuum (5100 Å).

3.5 NGC 7469

Similarly, we analysed the multifractal behaviours of the long-term optical light curves (i.e. the continuum at 5100 Å and the Hβ line) of NGC 7469. We present the results of our multifractality analysis in Fig. 9. We take into account the effects of observational noise on the widths and shapes of the spectra in the same way as for previous objects. Despite the spectral shapes remaining the same, we found small differences in the widths of the spectra. These small differences allowed us to obtain the 1σ errors (see Table 1). As can easily be seen, for the continuum (5100 Å), there is no difference in the behaviour of $Fq(n)$ for positive and negative q, and consequently $h(q)$ and $\tau(q)$ show linear dependence on q. Furthermore, the linearity in $h(q)$ and $\tau(q)$ is strengthened by the narrow spectral width $\Delta\alpha$. Similarly, for the Hβ line, the very weak dependence of $h(q)$ and $\tau(q)$ on q and the almost narrow spectral width indicate the presence of very weak multifractal (nearly monofractal) signatures in the time series of the Hβ line. Despite the narrow spectral widths, the differences in the width, $\Delta\alpha$(Hβ) > $\Delta\alpha$ (5100Å), could tell us something important about the relationship between the two light curves.

3.6 Partial observation period

We take into account the effects of the number of observations on the spectral width by considering an equal number of data points for all objects. We take the data points from day 50094.5 to day 52237.6 for NGC 4151 (5100 Å) and from day 50094.5 to day 52397.7 for NGC 4151 (Hβ), from day 50940.34 to day 55367.42 for Arp 102B (5100 Å and Hβ), from day 49832.42 to day 54040.65 for 3C 390.3 (5100 Å and Hβ), from day 50866.6 to day 55866.2 for E1821+643 (5100 Å and Hβ), and from day 50247.56 to day 52619.67 for NGC 7469 (5100 Å and Hβ). In this case, the maximum scale given by $n_{\max} = \text{round}\{\text{length}[x(t)]/10\}$, where $x(t)$ is the signal, which is

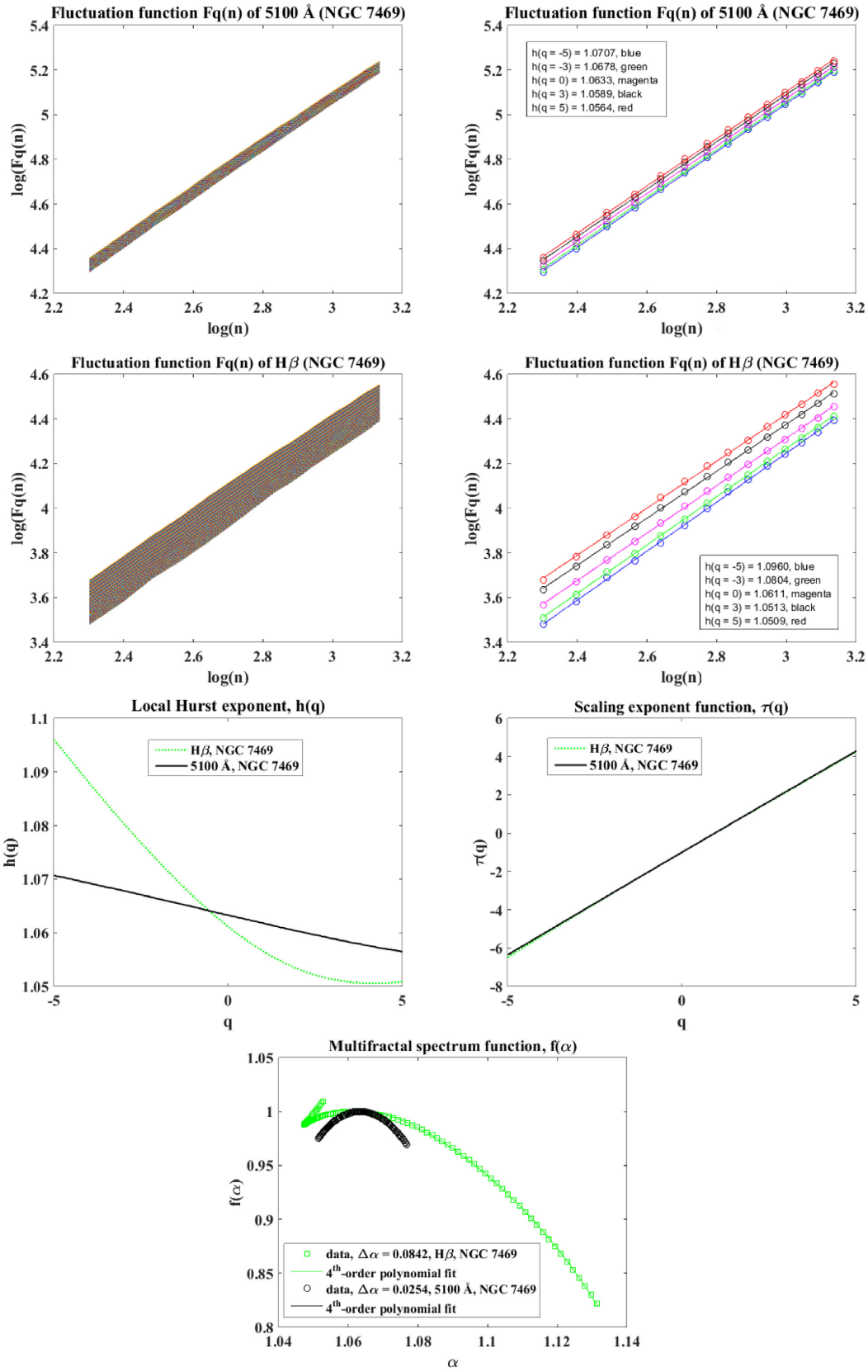

Figure 9. Top panels: the overall fluctuation functions $Fq(n)$ (left) and the fitted overall fluctuation functions for different Hurst exponents denoted with different colours (right) for the continuum of NGC 7469. First middle panels: the same as the top panels but for the Hβ line. Second middle panels: the local Hurst exponents $h(q)$ (left) for the continuum (black solid line) and Hβ line (green dots) and the scaling exponent functions $\tau(q)$ (right) for the continuum (black solid line) and Hβ line (green dots). Bottom panel: the multifractal spectrum functions for the observed continuum (black circle) and Hβ line (green square) fitted with a fourth-order polynomial function (solid lines). The width $\Delta\alpha$ of both spectrum functions is also given.

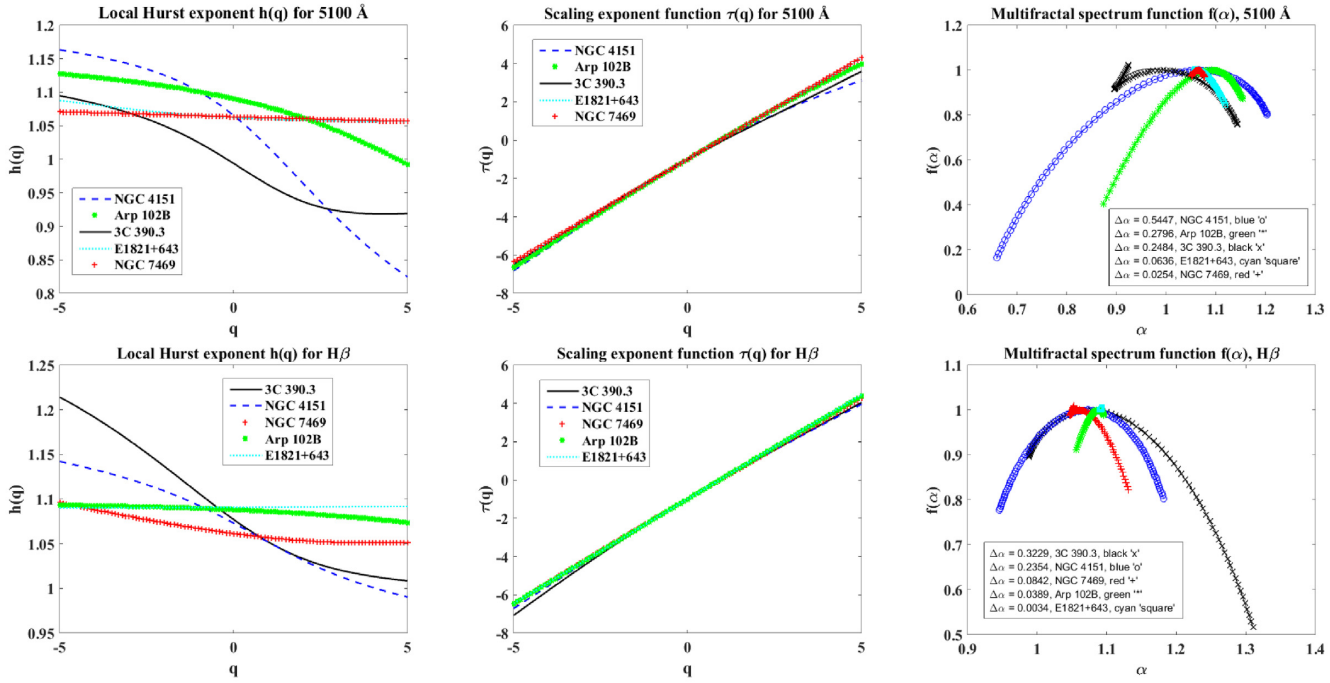

Figure 10. Top panels: comparisons among the local Hurst exponents $h(q)$ (left), scaling exponent functions $\tau(q)$ (middle) and multifractal spectrum functions $f(\alpha)$ (right) for the continuum (5100 Å) of the five objects for the full observation period. Bottom panels: the same as the top panels but for the Hβ line.

the same for all sources. Then, we repeated the same multifractality analysis for the light curves over these partial observation periods. The resulting local Hurst exponents $h(q)$, scaling exponent functions $\tau(q)$ and multifractal spectrum functions $f(\alpha)$ for the continuum and the Hβ line of all five objects are given in Fig. 10 for the full observation period (these can be compared with the results in Fig. 11 for the partial observation periods). The difference in the behaviours of $h(q)$ and $\tau(q)$ as a function of q between the emission line (Hβ) and continuum (5100 Å) of each object, as well as between the objects, clearly demonstrates the difference in the degree of multifractality. To characterize this difference quantitatively, we estimated the multifractal spectrum function $f(\alpha)$ and calculated the corresponding spectral widths (see Table 1).

Additionally, for the Hβ line segments of Arp 102B and E18 21+643, in addition to the analysis for the full observation period, we performed the same analysis for the partial observation periods: from day 50940.34 to day 55367.42 for the Hβ line segments of Arp 102B, and from day 50866.6 to day 55866.2 for the Hβ line segments of E1821+643. The multifractality analysis results are depicted in the bottom panels of Fig. 5 (Arp 102B) and Fig. 8 (E1821+643). The corresponding spectral widths for the Hβ line segments of Arp 102B and E1821+643 are given in Table 1. Additionally, for the partial observation periods, a nearly monofractal signature is found in all the segments. Though the variability in the total and partial light curves is similar (see Table 1), we found differences in the spectral widths between the two periods, implying that these differences could be due to changes in underlying processes at different time intervals or could be due to other numerical artefacts.

3.7 Global perspective

Different multifractal signatures are detected for the continuum at 5100 Å, the Hβ line profile and the Hβ line segments. Considering the full observation period, the nuclei for which the degree of multifractality of the continuum is greater than that of the line, i.e. $\Delta\alpha$ (5100 Å) > $\Delta\alpha$ (Hβ), are NGC 4151, Arp 102B (host-galaxy-corrected) and E1821+643. In contrast, for 3C 390.3 and NGC 7469, the multifractality of the line is found to be stronger than that of the continuum, i.e. $\Delta\alpha$ (5100 Å) < $\Delta\alpha$ (Hβ). The same is true for the partial observation periods, except for that of NGC 4151. For NGC 4151, it is worth noting that the multifractality of the continuum drastically decreases when we consider the partial observing period. In addition, we compared the degrees of multifractality of the continuum and the Hβ line between objects. For the continuum (5100 Å), $\Delta\alpha$ (NGC 4151) > $\Delta\alpha$ (Arp 102B) > $\Delta\alpha$ (3C 390.3) > $\Delta\alpha$ (E1821+643) > $\Delta\alpha$ (NGC 7469), whereas for the Hβ line, $\Delta\alpha$ (3C 390.3) > $\Delta\alpha$ (NGC 4151) > $\Delta\alpha$ (NGC 7469) > $\Delta\alpha$ (Arp 102B) > $\Delta\alpha$ (E1821+643). Additionally, for the partial observation periods containing an equal number of epochs, the order of the sources is the same despite the differences in their spectral widths (see Fig. 11). In all cases, for Arp 102B, we considered host-galaxy-corrected data for both the continuum and the line. We also compared the degrees of multifractality along the Hβ line profiles of Arp 102B and E1821+643, obtaining $\Delta\alpha_{\rm blue} > \Delta\alpha_{\rm core} \sim \Delta\alpha_{\rm red}$. However, when partial light curves are considered, the degree of multifractality slightly increases in E1821+643 but decreases in Arp102B. The changing behaviours of the multifractal signatures with the observation period could be due to the complex nature of both the central compact source (from where the ionizing continuum originates) and the BLR (from where the BELs are generated). We further investigated how the degree of multifractality depends on different physical properties of the considered AGN. In this analysis, we considered the results of the full observation period. The degree of multifractality of the continuum is found to be independent of the black hole mass and the continuum luminosity (see the top-left and top-middle panels of Fig. 12). However, excluding NGC 7469, the degree of multifractality seems

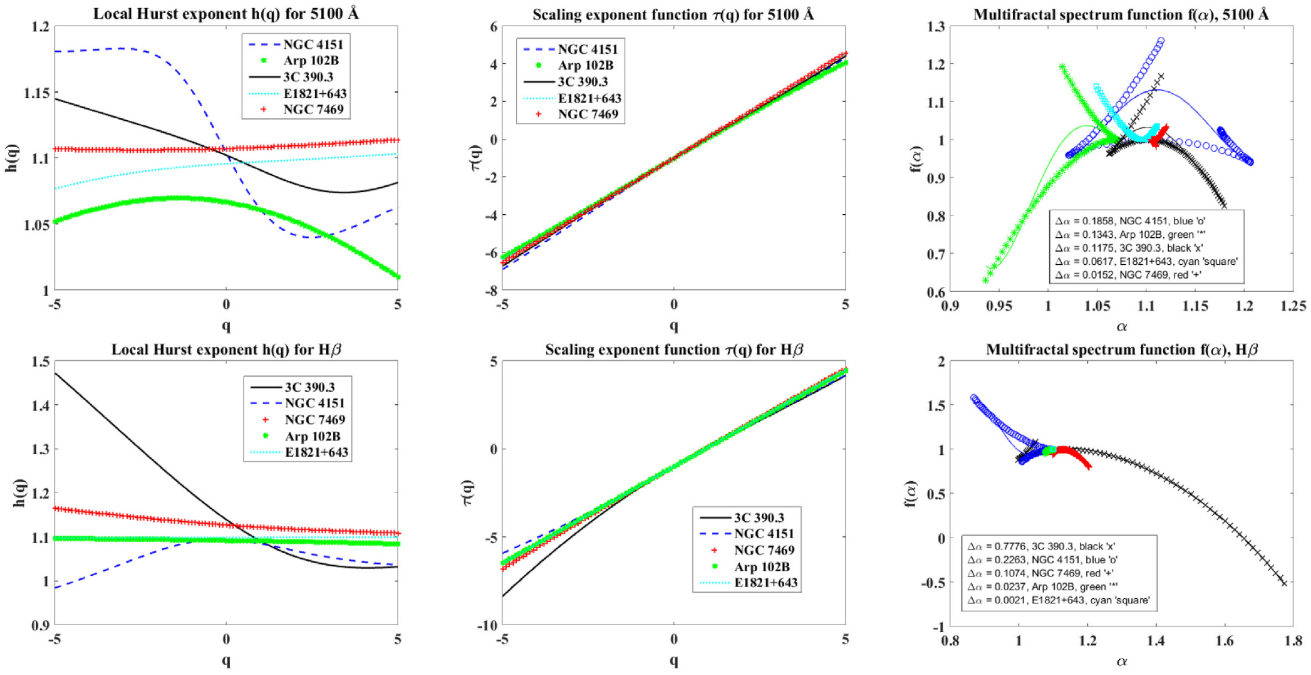

Figure 11. Top panels: comparisons among the local Hurst exponents $h(q)$ (left), scaling exponent functions $\tau(q)$ (middle) and multifractal spectrum functions $f(\alpha)$ (right) for the continuum (5100 Å) of the five objects for the partial observation period. Bottom panels: the same as the top panels but for the Hβ line.

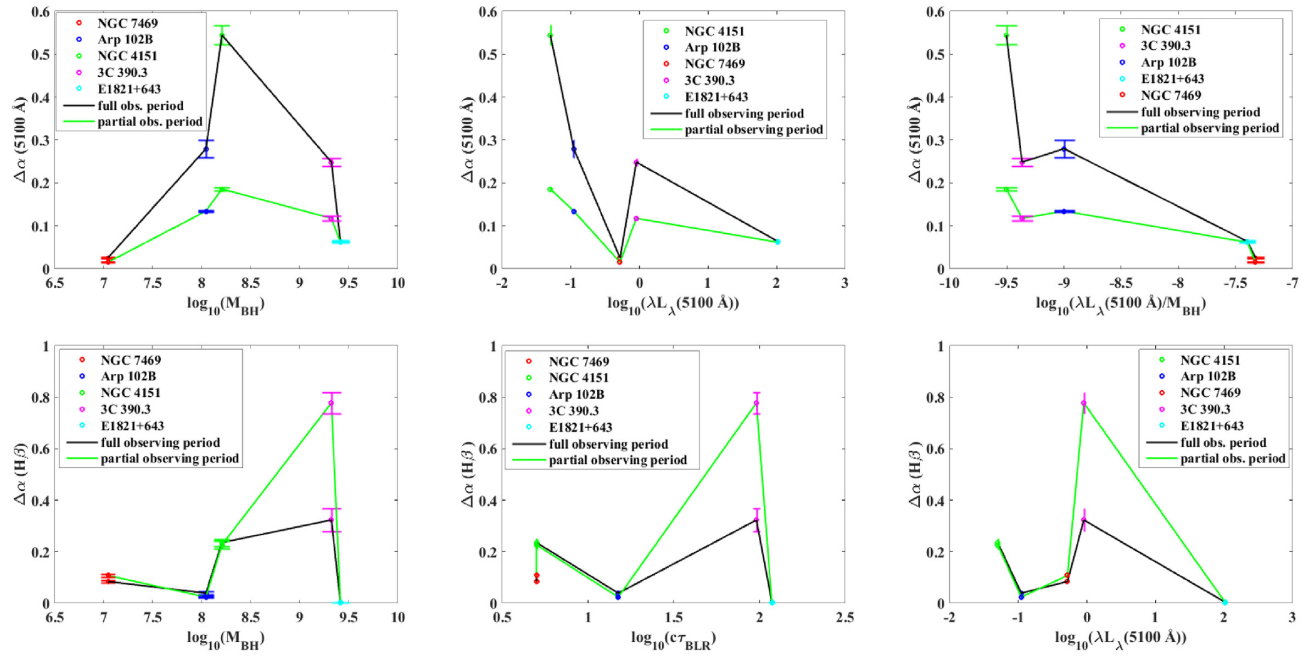

Figure 12. Top panels: $\Delta\alpha$ (5100 Å) versus black hole mass (left), $\Delta\alpha$ (5100 Å) versus mean continuum luminosity (middle) and $\Delta\alpha$ (5100 Å) versus $L_{\rm cont}/M_{\rm BH}$ (right). Bottom panels: $\Delta\alpha$ (Hβ) versus black hole mass (left), $\Delta\alpha$ (Hβ) versus radius of the BLR (middle) and $\Delta\alpha$ (Hβ) versus λL_λ(5100 Å) (right).

to be correlated with the continuum luminosity. Additionally, in the top-right panel of Fig. 12, we present the relationship between the degree of multifractality for the continuum flux and the λL_λ (5100 Å)/$M_{\rm BH}$ ratio, showing the presence of a possible correlation between them. The very interesting result of the drastic decrease of continuum light curve multifractality of NGC 4151, when the partial period is considered, could be related to the difference in the mean flux and mean luminosity between the total and partial period. In the partial period, the mean flux and luminosity are higher than those in the total period (see the top-left panel of Fig. 1), so that an appreciable increase in luminosity and Eddington ratio might lead to a significant decrease in the multifractal degree, as suggested by our global results in Fig. 12 (top-right panel). We also show that $\Delta\alpha$ of the Hβ line is not correlated with the

black hole mass or the radius of the BLR (see the bottom-left and bottom-middle panels in Fig. 12), which is in agreement with the results reported in Ilić et al. (2017). Moreover, $\Delta\alpha$ (Hβ) is also not correlated with the continuum luminosity (see the bottom-right panel in Fig. 12). Indeed, different Seyfert galaxies characterized by different rates of variability, different line profiles and, perhaps, different dynamics show different degrees of multifractality, and there is some indication that stronger variability is needed to detect multifractal signals. More analyses of the properties and dependence of the degree of multifractality on the observational properties of AGN light curves will be given elsewhere.

4 DISCUSSION AND CONCLUSIONS

In this work, for the first time, we present multifractality (non-linearity) analyses of the long-term optical light curves (i.e. the continuum at 5100 Å and the Hβ line) of selected type 1 AGNs: NGC 4151, Arp 102B, 3C 390.3, E1821+643 and NGC 7469. We used the backward ($\theta = 0$) one-dimensional MFDMA data analysis procedure. The overall fluctuation function $Fq(n)$, the local Hurst exponent $h(q)$, the classic scaling exponent function $\tau(q)$ and the multifractal spectrum function $f(\alpha)$ are essential tools for finding multifractal signatures. Thus, we estimated all these functions for each considered time series.

We detected multifractal signatures in the continua (5100 Å) of NGC 4151, Arp 102B and 3C 390.3 and in the Hβ lines of NGC 4151 and 3C 390.3, confirming once again that AGNs are non-linear, complex and intermittent systems (e.g. Vio et al. 1991; Longo et al. 1996; Bewketu Belete et al. 2018, 2019b) that cannot be fully described by a single power exponent or linear model. In the continua of E1821+643 and NGC 7469 and in the Hβ lines of Arp 102B, E1821+643 and NGC 7469, nearly monofractal (if not monofractal) signatures were detected. In addition, we also detected very weak multifractal (nearly monofractal) signatures in most Hβ line segments of Arp 102B and E1821+643. Interestingly, there is evidence that multifractality is playing a role in the light curve of the blue wing of the Hβ emission from Arp 102B, but it should be noted that it almost completely disappears when a partial observing period is considered, which is better sampled than the full observing period. The degree of multifractality was found to be different between the continuum and emission line of each individual object and between objects. Considering the full observation period, we found that the BLR smooths out the non-linearity of the continuum for NGC 4151, Arp 102B and E1821+643, whereas the Hβ emission signal has higher non-linearity than the continuum signal for 3C 390.3 and NGC 7469. Similarly, considering the partial observation periods containing an equal number of epochs, we found that the non-linearity of the continuum is greater than that of the line for Arp 102B and E1821+643, whereas the non-linearity of the continuum is less than that of the line for NGC 4151, 3C 390.3 and NGC 7469. We also discovered significant differences in the spectral widths for NGC 4151, Arp 102B and 3C 390.3 when we compared the results for the full observation period with those for the partial observation periods. The spectral widths of the partial observation periods usually decrease, except for the Hβ light curve of 3C 390.3, for which the width increases. In addition, for NGC 4151 and Arp 102B, we noticed that with a change in the considered period (full or partial), the degree of multifractality of the line decreases when the multifractality of the continuum decreases, implying the presence of possible correlations between the degrees of multifractality. We also found similar correlation behaviours between the continuum (5100 Å) and Hβ line of NGC 5548 (Bewketu Belete et al. 2019c). Kovačević et al. (2018) reported the presence of correlations in the oscillatory behaviours of the continuum and emission lines of NGC 4151, 3C 390.3, NGC 5548 and E1821+643, indicating that such correlations could be the consequence of a more general correlation trend between the continuum and emission-line fluxes of these sources. Comparing the degrees of multifractality between objects, for the continuum, the order from the strongest to the weakest in terms of the degree of multifractality is NGC 4151 > Arp 102B (host-galaxy-corrected) > 3C 390.3 > E1821+643 > NGC 7469, whereas for the Hβ line, the order is 3C 390.3 > NGC 4151 > NGC 7469 > Arp 102B (host-galaxy-corrected) > E1821+643.

These differences in the degree of multifractality and thus non-linearity between the AGNs might be a result of the differences in their dynamics. Kovačević et al. (2018) studied the oscillatory patterns in the continuum and emission-line variations of NGC 4151, Arp 102B, 3C 390.3, E1821+643 and NGC 5548; this small sample of AGNs includes four out of our five objects in addition to a Sy 1 nucleus whose spectral multifractality was analysed in a previous paper (NGC 5548; Bewketu Belete et al. 2019c). Regarding the two double-peaked Balmer line emitters (i.e. 3C 390.3 and Arp 102B), Kovačević et al. (2018) reported evidence that both objects have different dynamics and showed that the oscillations of NGC 5548 and E1821+643 correspond to the dynamical extremes of chaos and stability, respectively. Additionally, it has been shown that the rate of variability of 3C 390.3 is higher than that of Arp 102B and has a typical line variability that can be explained by disc emission and perturbations in the disc, whereas this characteristic is not seen in Arp 102B (Rakić et al. 2017, and references therein). Moreover, Rakić et al. (2017) described the differences in the spectral properties of galaxies 3C 390.3 and Arp 102B and found that their differences are due to the different structures of their BLRs.

The degree of multifractality of the continuum (5100 Å) is shown to be independent of the black hole mass. However, except for NGC 7469, the degree of multifractality seems correlated with the mean continuum luminosity. Furthermore, a good correlation is also found between the degree of multifractality of the continuum and the λL_λ (5100 Å)/$M_{\rm BH}$ ratio (i.e. a tracer of the Eddington ratio $L/L_{\rm Edd}$), with higher multifractality at a lower ratio. Although this finding provides clues about a possible link between non-linearity and accretion physics (supermassive black holes and mass accretion rates), this relationship must be taken with caution because of the small size of our sample of AGNs. In addition, we found that the degree of multifractality of the Hβ line is independent of the black hole mass, the radius of the BLR and the mean continuum luminosity. We have also verified that the Hβ multifractality degree is not correlated with the λL_λ (5100 Å)/$M_{\rm BH}$ ratio. The Hβ lines of Arp 102B and E1821+643 exhibit a double-peaked or highly asymmetric profile, and thus the observed differences between the line regions of these two AGNs are worth discussing. There is an excess of multifractality in the blue wing of the emission line of Arp 102B only, so the degree of multifractality is higher for the BLR region moving towards Earth. Moreover, the motions of emitting clouds may affect both the amplitude and the time-scale of observed line flux variations; hence, different motions could produce differences in the nature (multifractality/non-linearity) of the corresponding signal.

It has been shown that the degree of multifractality does not change with redshift; that is, multifractality is an intrinsic behaviour of AGNs (Bewketu Belete et al. 2019b). However, extrinsic variations (e.g. microlensing effects) could affect the width of a multifractal spectrum (Bewketu Belete et al. 2019a). Thus, believing multifractality to be an intrinsic property of AGNs and assuming that

photoionization is the main source for the production of emission lines in AGNs, our results could provide significant information about the behaviours of the continua and BLRs of AGNs and whether the BLR smooths out the non-linearity of the continuum. It might be necessary to note this when cross-correlating the line and continuum light curves to estimate the size of the BLR, as the cross-correlation peak position depends on the nature of the continuum light curve and on the response of the emission lines (Netzer 1990). For example, based on our results, the response of the Hβ line to the variations in the continuum at 5100 Å is found to be linear (smoothed out) for Arp 102B, whereas the response is non-linear for 3C 390.3. There is ambiguity in the result for NGC 4151, because the situation depends on the time segment considered. Similarly, in our previous work (Bewketu Belete et al. 2019c), we performed the same multifractality analysis for long-term (1972–2015) optical continuum (5100 Å) and Hβ line observations of the Seyfert 1 galaxy NGC 5548 (Bon et al. 2016) and we found a non-linear response of the Hβ line to the variation in the continuum at 5100 Å.

We found multifractal signatures in half of the light curves considered. Nearly monofractal signatures were detected for the continua of E1821+643 and NGC 7469, as well as for the Hβ lines of Arp 102B, E1821+643 and NGC 7469; however, these behaviours may change during different analysed periods. Thus, additional and more frequent observations are needed; fortunately, large and dedicated surveys, both photometric and spectroscopic, such as the Panoramic Survey Telescope and Rapid Response System (Pan-STARRS), the Vera C. Rubin Observatory Legacy Survey of Space and Time (LSST), the Sloan Digital Sky Survey (SDSS) and the Maunakea Spectroscopic Explorer (MSE), will most definitely provide these data in the future. Interestingly, there is evidence that multifractality plays a role in the light curve of the blue wing of the Hβ line emission from Arp 102B. We did not find any correlations between the degree of multifractality of the Hβ line and the accretion parameters, although the degree of multifractality of the continuum may display some dependence on the Eddington ratio. In general, however, there is an important caveat regarding these encouraging results. The given method is not robust and independent of the sampling rate and other properties of the light curves. Thus, in future work, these limitations will be fully addressed through future long-term monitoring campaigns and/or with the analysis of artificial AGN light curves that are carefully generated with different approaches.

ACKNOWLEDGEMENTS

The research activities of the Observational Astronomy Board of the Federal University of Rio Grande do Norte (UFRN) are supported by continuous grants from the Brazilian National Council for Scientific and Technological Development (CNPq) and FAPERN in Brazil. We also acknowledge financial support from INCT INEspaço/CNPq/MCT. We sincerely thank the anonymous referee for valuable suggestions and comments that greatly improved this work. ABB acknowledges a CAPES PhD fellowship, and LJG acknowledges support from MINECO/AEI/FEDER-UE grant AYA2017-89815-P and the University of Cantabria.

REFERENCES

Alexander T., Sturm E., Lutz D., Sternberg A., Netzer H., Genzel R., 1999, ApJ, 512, 204
Antonucci R. R. J., Cohen R. D., 1983, ApJ, 271, 564
Antonucci R., Hurt T., Agol E., 1996, ApJ, 456, L25
Ashkenazy Y., Baker D. R., Gildor H., Havlin S., 2003, Geophys. Res. Lett., 30, 2146
Baldi R. D., Behar E., Laor A., Horesh A., 2015, MNRAS, 454, 4277
Barr P. et al., 1980, MNRAS, 193, 549
Beall J. H., Rose W. K., Dennis B. R., Crannell C. J., Dolan J. F., Frost K. J., Orwig L. E., 1981, ApJ, 247, 458
Bewketu Belete A., Bravo J. P., Canto Martins B. L., Leão I. C., De Araujo J. M., De Medeiros J. R., 2018, MNRAS, 478, 3976
Bewketu Belete A., Canto Martins B. L., Leão I. C., De Medeiros J. R., 2019a, MNRAS, 484, 3552
Bewketu Belete A., Femmam S., Tornikosk M., Lähteenmäki A., Tammi J., Leão I. C., Canto Martins B. L., De Medeiros J. R., 2019b, ApJ, 873, 108
Bewketu Belete A., Goicoechea L. J., Leão I. C., Martins B. L. C., Medeiros J. R. D., 2019c, ApJ, 879, 113
Blundell K. M., Rawlings S., 2001, ApJ, 562, L5
Bon E. et al., 2016, ApJS, 225, 29
Chen K., Halpern J. P., 1989, ApJ, 344, 115
Chen K., Halpern J. P., Filippenko A. V., 1989, ApJ, 339, 742
Chian A. C. L., 1997, in Wickramasinghe D. T., Bicknell G. V., Ferrario L., eds, ASP Conf. Ser. Vol. 121, IAU Colloq. 163: Accretion Phenomena and Related Outflows. Astron. Soc. Pac., San Francisco, CA, p. 663
Czerny B., Doroshenko V. T., Nikolajuk M., Schwarzenberg-Czerny A., Loska Z., Madejski G., 2003, MNRAS, 342, 1222
de Freitas D. B. et al., 2016, ApJ, 831, 87
de Freitas D. B., Nepomuceno M. M. F., Cordeiro J. G., Das Chagas M. L., De Medeiros J. R., 2019, MNRAS, 488, 3274
Dietrich M. et al., 1998, ApJS, 115, 185
Dietrich M. et al., 2012, ApJ, 757, 53
Doroshenko V., Sergeev S., Vovk E. Y., Efimov Y. S., Klimanov S., Nazarov S., 2010, Astron. Lett., 36, 611
Dultzin-Hacyan D., Schuster W. J., Parrao L., Pena J. H., Peniche R., Benitez E., Costero R., 1992, AJ, 103, 1769
Dultzin-Hacyan D., Ruelas-Mayorga A., Costero R., 1993, Rev. Mex. Astron. Astrofis., 25, 143
Edelson R. et al., 2019, ApJ, 870, 123
Fan J-H., Su C-Y., Lin R-G., 2002, PASJ, 54, 175
Gezari S., Halpern J. P., Eracleous M., Filippenko A. V., 2004, in Storchi-Bergmann T., Ho L. C., Schmitt H. R., eds, Proc. IAU Symp. Vol. 222, The Interplay Among Black Holes, Stars and ISM in Galactic Nuclei. Kluwer, Dordrecht, p. 95
Gezari S., Halpern J. P., Eracleous M., 2007, ApJS, 169, 167
Gu G-F., Zhou W-X., 2010, Phys. Rev. E, 82, 011136
Guo D., Tao J., Qian B., 2006, PASJ, 58, 503
Hampson K. M., Mallen E. A. H., 2011, Biomed. Opt. Express, 2, 464
Ihlen E., 2012, Frontiers in Physiology, 3, 141
Ilić D. et al., 2017, Frontiers in Astronomy and Space Sciences, 4, 12
Kantelhardt J. W., Zschiegner S. A., Koscielny-Bunde E., Havlin S., Bunde A., Stanley H. E., 2002, Physica A: Statistical Mechanics and its Applications, 316, 87
Kollatschny W., Zetzl M., Dietrich M., 2006, A&A, 454, 459
Kolman M., Halpern J. P., Shrader C. R., Filippenko A. V., 1991, ApJ, 373, 57
Kolman M., Halpern J. P., Shrader C. R., Filippenko A. V., Fink H. H., Schaeidt S. G., 1993, ApJ, 402, 514
Kovačević A., Popovic L. ., Shapovalova A. I., Ilic D., 2017, Ap&SS, 362, 31
Kovačević A. B., Pérez-Hernández E., Popović L. Č., Shapovalova A. I., Kollatschny W., Ilić D., 2018, MNRAS, 475, 2051
Landt H., Bentz M. C., Ward M. J., Elvis M., Peterson B. M., Korista K. T., Karovska M., 2008, ApJS, 174, 282
Longo G., Vio R., Paura P., Provenzale A., Rifatto A., 1996, A&A, 312, 424
Maoz D. et al., 1991, ApJ, 367, 493
Mehdipour M. et al., 2018, A&A, 615, A72
Middei R. et al., 2018, A&A, 615, A163
Netzer H., 1982, MNRAS, 198, 589

Netzer H., 1990, Active Galactic Nuclei. Springer, Berlin, p. 57
Newman J. A., Eracleous M., Filippenko A. V., Halpern J. P., 1997, ApJ, 485, 570
Oegerle W. et al., 2000, ApJ, 538, L23
Peterson B. M., 1993, PASP, 105, 247
Peterson B. M., 2014, Space Sci. Rev., 183, 253
Peterson B. et al., 2014, ApJ, 795, 149
Petrucci P., Maraschi L., Haardt F., Nandra K., 2004, A&A, 413, 477
Popović L. Č. et al., 2011, A&A, 528, A130
Popović L. Č. et al., 2014, A&A, 572, A66
Pronik S. G. S. V., Sergeeva E. A., 2001, ApJ, 554, 245
Rakić N., La Mura G., Ilić D., Shapovalova A. I., Kollatschny W., Rafanelli P., Popović L., 2017, A&A, 603, A49
Seifina E., Titarchuk L., Ugolkova L., 2018, A&A, 619, A21
Sergeev S. G., Pronik V. I., Peterson B. M., Sergeeva E. A., Zheng W., 2002, ApJ, 576, 660
Sergeev S. G., Klimanov S. A., Doroshenko V. T., Efimov Y. S., Nazarov S. V., Pronik V. I., 2011, MNRAS, 410, 1877
Sergeev S., Nazarov S., Borman G., 2017, MNRAS, 465, 1898
Shapovalova A. I., Burenkov A. N., Carrasco L., Chavushyan V. H., Doroshenko V. T., 2001, A&A, 376, 775
Shapovalova A. I. et al., 2008, A&A, 486, 99
Shapovalova A. I. et al., 2009, New Astron. Rev., 53, 191
Shapovalova A. I., Popović L. Č., Burenkov A. N., Chavushyan V. H., Ilić D., Kovačević A., Bochkarev N. G., León-Tavares J., 2010a, A&A, 509, A106
Shapovalova A. I. et al., 2010b, A&A, 517, A42
Shapovalova A. I. et al., 2013, A&A, 559, A10
Shapovalova A. I. et al., 2016, ApJS, 222, 25
Shapovalova A. I. et al., 2017, MNRAS, 466, 4759
Tanna H. J., Pathak K. N., 2014, Ap&SS, 350, 47
Tao J., Fan J., Qian B., Liu Y., 2008, AJ, 135, 737
Ulrich M.-H., 2000, A&AR, 10, 135
Veilleux S., Zheng W., 1991, ApJ, 377, 89
Vio R., Cristiani S., Lessi O., Salvadori L., 1991, ApJ, 380, 351
Vio R., Cristiani S., Lessi O., Provenzale A., 1992, ApJ, 391, 518
Walker S., Fabian A., Russell H., Sanders J., 2014, MNRAS, 442, 2809
Wamsteker W., Wang T-G., Schartel N., Vio R., 1997, MNRAS, 288, 225
Wang Y., Wu C., Pan Z., 2011, Physica A: Statistical Mechanics and its Applications, 390, 3512
Welsh W., Peterson B., Koratkar A., Korista K., 1998, ApJ, 509, 118
Yee H. K. C., Oke J. B., 1981, ApJ, 248, 472
Zheng W., 1996, AJ, 111, 1498

This paper has been typeset from a TEX/LATEX file prepared by the author.